# AERIAL IMAGES AND LIDAR DATA FUSION FOR AUTOMATIC FEATURE EXTRACTION USING THE SELF-ORGANIZING MAP (SOM) CLASSIFIER

M. Salah [a, *], J.Trinder [a], A.Shaker [b], M.Hamed[b], A.Elsagheer [b]

[a] School of Surveying and Spatial Information Systems, The University of New South Wales,
UNSW SYDNEY NSW 2052, Australia - (m.gomah, j.trinder)@unsw.edu.au
[b] Dept. of Surveying, Faculty of Engineering Shoubra, Benha University, 108 Shoubra Street, Cairo, Egypt -
ahmshaker@link.net, prof.mahmoudhamed@ yahoo.com, alielsagheer@yahoo.com

**KEY WORDS:** Aerial Images, Lidar, GLCM, Attributes, Building Detection, Classification, Self-Organizing Map.

**ABSTRACT:**

This paper presents work on the development of automatic feature extraction from multispectral aerial images and lidar data based on test data from two different study areas with different characteristics. First, we filtered the lidar point clouds to generate a Digital Terrain Model (DTM) using a novel filtering technique based on a linear first-order equation which describes a tilted plane surface, and then the Digital Surface Model (DSM) and the Normalised Digital Surface Model (nDSM) were generated. After that a total of 22 uncorrelated feature attributes have been generated from the aerial images, the lidar intensity image, DSM and nDSM. The attributes include those derived from the Grey Level Co-occurrence Matrix (GLCM), Normalized Difference Vegetation Indices (NDVI) and slope. Finally, a SOM was used to detect buildings, trees, roads and grass from the aerial image, lidar data and the generated attributes. The results show that using lidar data in the SOM improves the accuracy of feature detection by 38% compared with using aerial photography alone, while using the generated attributes as well improve the detection results by a further 10%. The results also show that the following attributes contributed most significantly to detection of buildings, trees, roads and grass respectively: entropy (from GLCM) derived from nDSM; slope derived from nDSM; homogeneity (from the GLCM) derived from nDSM; and homogeneity derived from nDSM.

## 1. INTRODUCTION

Research on automated feature extraction from aerial images and lidar data has been fuelled in recent years by the need for data acquisition and updating for GIS. The high dimensionality of aerial and satellite imagery presents a challenge for traditional classification methods based on statistical assumptions. Artificial Neural Networks (ANNs) on the other hand may represent a valuable alternative approach for land cover mapping for such highly dimensional imagery. ANNs require no assumption regarding the statistical distribution of the input pattern classes (Hugo *et al.*, 2007) and they have two important properties: the ability to *learn* from input data; and to generalize and predict unseen patterns based on the data source, rather than on any particular *a priori* model. The Self-Organizing Map is one of the most commonly used neural network classifiers. It can be adjusted to adapt to the probability distribution of the inputs (Seto and Liu, 2003).

In this paper we applied the SOM algorithm for combining multispectral aerial imagery and lidar data so that the individual strengths of each data source can compensate for the weakness of the other. The low contrast, occlusions and shadow effects in the image were compensated by the accurately detected planes in the lidar data. However, edges of features are not located accurately in lidar point clouds because of the lidar's system discrete sampling interval of 0.5m to 1m, (Li and Wu, 2008). Therefore, we have derived 22 attributes from both aerial image and lidar data by a number of algorithms to alleviate this problem. To evaluate the contribution of the lidar data and the generated attributes in the detection process, three separate

SOM classification tests were carried out using different input data to determine the accuracy of feature detection against a reference map:

1. The aerial image, the lidar data and the derived attributes,
2. The aerial image and the lidar data,
3. The aerial image only as input data for the SOM.

Finally, the contributions of the individual attributes to the quality of the classification results were evaluated.

## 2. RELATED WORK

There have been many research efforts on the application of aerial images and lidar data for building extraction. Rottensteiner *et al.,* (2005) evaluated a method for building detection by the Dempster-Shafer fusion of lidar data and multispectral images. The heuristic model for the probability mass assignments for the method was validated, and rules for tuning the parameters of this model were discussed. Further, they evaluated the contributions of the individual cues used in the classification process to the quality of the classification results, which showed that the overall correctness of the results can be improved by fusing lidar data with multispectral images.

Matikainen *et al.,* (2007) used a classification tree approach for building detection. A digital surface model (DSM) derived from last pulse laser scanner data was first segmented into classes 'ground' and 'building or tree'. Different combinations of 44

---
* Corresponding author.

input attributes were used. The attributes were derived from the last pulse DSM, first pulse DSM and a colour aerial ortho image. In addition, shape attributes calculated for the segments were used. Compared with a building reference map, a mean accuracy of almost 90% was achieved for extracting buildings.

The numbers of studies that have utilized ANNs for highly spectrally dimensional image analysis are limited. Jen-Hon and Din-Chang (2000) applied the self-organized map classification (SOM) method for SPOT scene land cover classification. Hugo *et al.* (2007) assessed the potential of the SOM neural network to extract complex land cover information from medium resolution satellite imagery using MERIS Full Resolution data.

## 3. STUDY AREA AND DATA SOURCES

Two test data sets of different characteristics were used in this study. The first area is a part of the University of New South Wales campus; Sydney Australia, covering approximately 500m x 500m. It is a largely urban area that contains residential buildings, large Campus buildings, a network of main roads as well as minor roads, trees and green areas. Lidar data were acquired over the study area in April 2005, using an Optech ALTM 1225 with a pulse repetition frequency (PRF) of 25kHz at a wavelength of 1.047μm. The multispectral imagery was captured by film camera by AAMHatch on June 2005 at 1:6000 scale. The film was scanned in three colour bands (red, green and blue) in TIFF format, with 15μm pixel size (GSD of 0.09m) and radiometric resolution of 16-bit as shown in Figure 1(left).

The second study area is a part of Bathurst city; NSW Australia, covering approximately 1000m x 1000m. It is a largely rural area that contains small sized residential buildings, road networks, trees and green areas. Lidar data was acquired over the area by a Leica ALS50 sensor in August 2008, operating with a PRF of 150kHz at a wavelength of 1.064μm. The multi-spectral imagery was captured by a Leica ADS40 sensor on October 2007. Three colour band (red, green and blue) images were collected at 50cm GSD as shown in Figure 1(right).



Figure 1. Orthophotos for UNSW (left), Bathurst (right).

## 4. METHODOLOGY

Feature extraction of the study area was implemented in several stages as follow:

### 4.1 Filtering of lidar point clouds

Filtering is the process of separating on-terrain points (DTM) from points falling onto natural and human made objects. Axelsson (2000) developed an adaptive Triangulated Irregular Network (TIN) method to find ground points based on selected seed ground measurements. Whitman *et al.,* (2003) used an elevation threshold and an expanding search window to remove

non-ground points. Abo Akel *et al.,* (2004) used a robust method with orthogonal polynomials and road network for filtering of lidar data in urban areas.

The basic assumption of the approach adopted in this paper is that the height of a ground point is lower than the heights of neighbouring non-ground points and the terrain can be described using a simple tilted plane within small areas. The method started by dividing the data into small 50m x 50m square patches. In principle, the patch should be larger than the largest building within the test area in such a way that no object within the study area can totally cover the patch. Otherwise, points falling over buildings will be classified as on-terrain points. Then, the algorithm constructed a matrix, A (m, n), where m and n are the number of patches in both X and Y directions respectively, see figure 2(left). Then, the lower left and the upper right coordinates for each patch were determined and stored. Data from both the first and the last pulse echoes were used in order to obtain denser terrain data and hence a more accurate filtering process. For each patch we fitted tilted plane surfaces to the terrain points using equation (1):

$$Z = a + b * x + c \qquad (1)$$

where    X, Y and Z = coordinates of lidar point clouds.

The process of plane surface construction started with the detection of two points, one on each patch border, in the Y direction, which represent the minimum elevations on these borders. The two points were then shifted in X directions by a reasonable value, for example 1000m, while Z values remained constant, see figure 2(middle). The reason behind the shifting process is to create a new set of two points to construct a comparison plane, see figure 2(right), which includes the four detected points (two old and two new) and represents the general slope of the patch. The main assumption here was that the surface varies slowly from region to region over the patch of interest. The four points were then used to determine the best estimates of the coefficients of the plane by a least squares solution. Based on the computed coefficient values of a, b and c, equation (1) was applied for each individual point i with coordinates $X_i$, $Y_i$ in the lidar point clouds to find the Z value of its corresponding point on the plane. From a comparison of the elevation of each data point with its corresponding elevation on the generated plane surface, all points below, on or above this plane within the threshold t (=15cm), were classified as on-terrain points.  Threshold t was equal to the lidar system accuracy. Figure 2 demonstrates the steps of the filtering process, while figure 3 shows a part of the results for UNSW data.
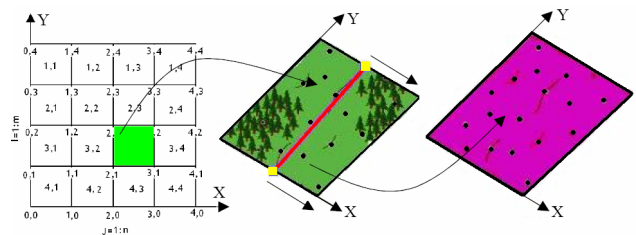


Figure 2.  Dividing the area into small square patches (left), detecting and shifting the lowest two points of the patch (middle) and constructing the tilted plane and removing the non-ground features (right).
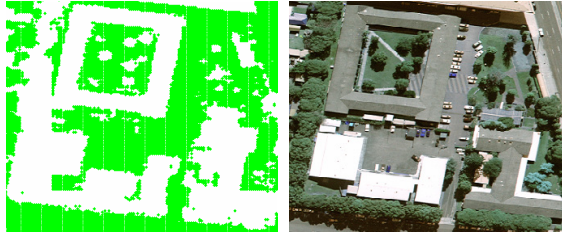
Figure 3. Points filtered as on-terrain points in green colour (left) compared to the aerial image (right).

Finally, the filtered lidar points were converted into an image DTM, the DSM was generated from the original Lidar point clouds (first and last pulses) and the nDSM was generated by subtracting the DTM from the DSM, see figures 4. These are grey scale images where tones range from dark for low elevations to bright for high elevations.
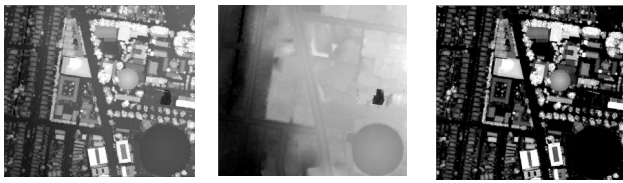


Figure 4. DSM (left), DTM (middle) and the nDSM (right).

In order to analyze the produced filtering errors, a sample of 100 well distributed filtered points has been selected, overlaid on the orthophoto and classified visually as ground and non-ground. Compared to those results, our algorithm has achieved commission errors, classifying non-ground points as ground points, and omission errors, classifying ground points as non-ground points, of about 3.1% and 5.2% for UNSW case study and 5.9% and 9.4% respectively for Bathurst case study. Compared with other methods, this technique is simple and requires no work tuning parameters except for the patch size. Also, fitting a simple tilted plane into a small square area effectively removes most of the non-ground points especially those on low vegetation.

## 4.2 Generation of attributes

Features or attributes commonly used for feature extraction from aerial images and lidar data include height texture (Maas and Vosselman, 1999) or surface roughness (Brunn and Weidner, 1998) of the lidar data, reflectance information from aerial images (Vögtle and Steinle, 2000) or lidar data (Hug, 1997), the difference between first and last pulses of the lidar data (Alharthy and Bethel, 2002). The attributes calculated for predefined segments or single pixels are presented as input data for a classification method. Before generating the attributes, the aerial photographs (already orthorectified by AAMHatch) were registered to the lidar intensity image using a projective transformation. The Root Mean Square (RMS) errors from the modelling process were 0.01m and 0.01m in X and Y respectively and the total RMS error was 0.02m, indicating an accurate registration between image and lidar data and demonstrating that most of the geometric distortions had already been removed by the orthorectification process. Following the transformation, the image was resampled to 30cm x 30cm and 50cm x 50cm cell size in case of UNSW and Bathurst respectively to match the resolution of the lidar data. A bilinear interpolation was used for resampling, which results in a better quality image than nearest neighbour resampling and requires less processing than cubic convolution.

In our test, a set of 78 possible attributes were selected as shown in Table 1. Because of the way the texture equations derived from the GLCM (Haralick, 1979) are constructed, many of them are strongly correlated with one another. Clausi (2002) analysed the correlations among the texture measures to determine the best subset of measures and showed that Contrast, Correlation and Entropy used together outperformed any one of them alone. If only one can be used, he recommended choosing from amongst Contrast, Dissimilarity or Homogeneity. Based on these experiments, only 22 of the 78 possible attributes were uncorrelated and hence available for the classification process as shown in the shaded cells of Table 1. The attributes include those derived from the GLCM, Normalized Difference Vegetation Indices (NDVI), standard deviation of elevations, slope and the polymorphic texture strength based on the Förstner operator (Förstner and Gülch, 1987).

| Attributes | Attribute | R | G | B | I | DSM | NDSM |
|---|---|---|---|---|---|---|---|
| Spectral | Mean | ● | ● | ● | ● | ● | ● |
| | St. Deviation | ● | ● | ● | ● | ● | ● |
| GLCM | Strength | ● | ● | ● | ● | ● | ● |
| | Contrast | ● | ● | ● | ● | ● | ● |
| | Dissimilarity | ● | ● | ● | ● | ● | ● |
| | Homogeneity | ● | ● | ● | ● | ● | ● |
| | A.S.M | ● | ● | ● | ● | ● | ● |
| | Entropy | ● | ● | ● | ● | ● | ● |
| | Mean | ● | ● | ● | ● | ● | ● |
| | Variance | ● | ● | ● | ● | ● | ● |
| | Correlation | ● | ● | ● | ● | ● | ● |
| Height | SD | ● | ● | ● | ● | ● | ● |
| | Slope | ● | ● | ● | ● | ● | ● |

Table 1. The full set of the attributes; attributes available for the classification are shown by shading.

## 4.3 Land cover classification

The SOM (Kohonen, 1999) was used for classifying the images. Figure 5 illustrates the basic architecture of an SOM. The input layer represents the input feature vector and thus has neurons for each measurement dimension. In our study, we applied a separate neuron for each band. Therefore, the SOM has 29 input neurons which are: 22 generated attributes, 3 image bands (R, G and B), intensity image, DTM, DSM and nDSM. For the output layer of an SOM, we used a 15 x 15 array of neurons as an output for the SOM. This number was selected because, as recommended by Hugo *et al.* (2007), small networks result in some unrepresented classes in the final labelled network, while large networks lead to an improvement in the overall classification accuracy. Each output layer neuron is connected to all neurons in the input layer by synaptic weights.
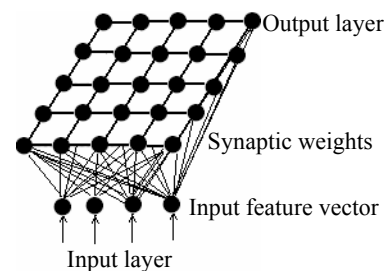


Figure 5. Example of SOM with a 4 neurons input layer and an equally spaced 5x5 neurons output layer.

During the training period, each neuron with a positive activity within the neighbourhood of the winning neuron participates in the learning process. A winning processing element is determined for each input vector based on the similarity between the input vector and the weight vector (Jen-Hon and Din-Chang, 2000). Let X= $(x_1, x_2, x_3..., x_n)$ be a vector of reflectances for a single pixel input to the SOM. We took the previously mentioned 29 values (22 generated attributes, 3 image bands, R, G and B, intensity image, DTM, DSM and nDSM) as the vector of reflectances of each pixel. Initially, synaptic weights between the output and input neurons were randomly assigned (0-1). The weight vector, $W_{ji}$, corresponding to output layer neuron j can be written as in equation (2):

$$w_{ji} = [w_{j1} \ w_{j2} \ ....... \ w_{jp}]^T \qquad j = 1, 2, 3, ..., N \qquad (2)$$

The distances between a weight vector and an input feature vector were then calculated, and the neuron in the output layer with the minimum distance to the input feature vector (known as the winner) was then determined as in equation (3):

$$winner = \arg\min\left(\sum_{i=1}^{n}(x_i^t - w_{ji}^t)^2\right) \qquad (3)$$

Where    $x_i^t$ = the input to neuron i at iteration t

$w_{ji}^t$ = the synaptic weight from input neuron i to output neuron j at iteration t.

The weight of the winner and its neighbours within a radius $\gamma$ were then altered (while those outside were left unaltered) according to a learning rate $\alpha^t$ as shown in equations (4, 5):

$$w_{ji}^{t+1} = w_{ji}^t + \alpha^t(x_i^t - w_{ji}^t), \ \forall d_{winner\ j} \in \gamma^t \qquad (4)$$

$$w_{ji}^{t+1} = w_{ji}^t, \ \forall d_{winner\ j} \notin \gamma^t \qquad (5)$$

where    $\alpha^t$ = the learning rate at iteration t

$d_{winner\ j}$ = the distance between the winner and other neurons in the output layer.

$\alpha^t$ was calculated from equation (6):

$$\alpha^t = \alpha_{max}\left(\frac{\alpha_{min}}{\alpha_{max}}\right)^{\frac{1}{t}} \qquad (6)$$

The parameter values for our test were selected according to the suggestions proposed by Vesanto et al. (2000) to improve the classification accuracy without giving any computer memory constrains, see table 2. Figure 6 shows the classification results.

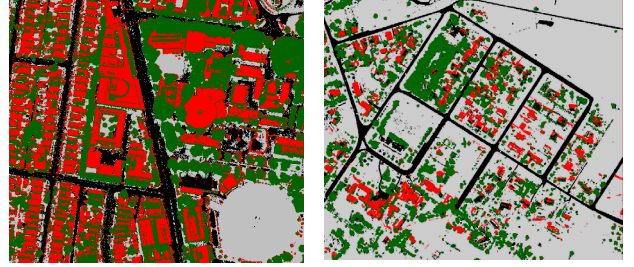| Input Neurons | Out put neurons | Initial $\gamma$ | Min. $\alpha$ | Max. $\alpha$ |
|---|---|---|---|---|
| 22 | 225 (15*15) | 25 | 0.5 | 1 |

Table 2. SOM parameters used for the test.



Figure 6. Results of the SOM classification for UNSW (left) and Bathurst (right). Red: buildings, green: trees, black: roads and grey: grass.

## 5.   RESULTS AND ANALYSIS

### 5.1   Evaluation of the classification results

To evaluate the contribution of lidar data and attributes to the classification accuracy, the SOM was performed three times. By using the aerial image alone on the UNSW data, many buildings were classified as roads because they have the same spectral reflectance and the classification accuracy was 49% (Figure 7b). The use of the lidar data along with the aerial image increased the classification accuracy to about 87% due to its ability to detect planes accurately but still some errors occurred due to the poor horizontal accuracy of edge detection in the lidar data (Li and Wu, 2008) (Figure 7c). The use of the UNSW aerial imagery, lidar data and extracted attributes improved the classification accuracy again to about 98% since the attributes compensated for the weakness of lidar for edge detection (Figure 7d). The classification accuracies for the Bathurst case study for the three different cases were 52%, 85% and 94% respectively.
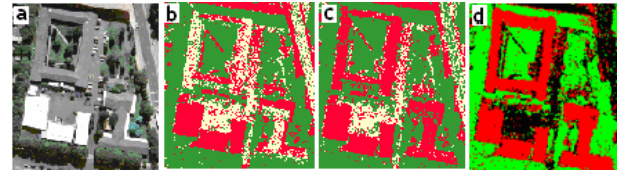


Figure 7. For UNSW data (a) The multispectral aerial image, (b) The SOM classified image using aerial image only, (c) The SOM classified image using aerial image and lidar data, (d) The SOM classified image using aerial image, lidar data and attributes.

### 5.2   Contributions of the individual attributes

Furthermore, we evaluated the contributions of the individual attributes to the quality of the classification results. The red, green and blue bands of the aerial image were considered as the primary data source and were available in each test. Figure 8 shows that: intensity image and entropy derived from nDSM performed best for building detection with 73% and 83% average classification accuracies respectively; homogeneity, strength and slope derived from nDSM performed best for tree detection with 82%, 82% and 86% average classification accuracies respectively; nDSM, entropy and homogeneity

derived from nDSM performed best for road detection with 94%, 95% and 97% average classification accuracies respectively; intensity image and entropy and homogeneity derived from nDSM performed best for grass detection with 68%, 72% and 77% average classification accuracies respectively.
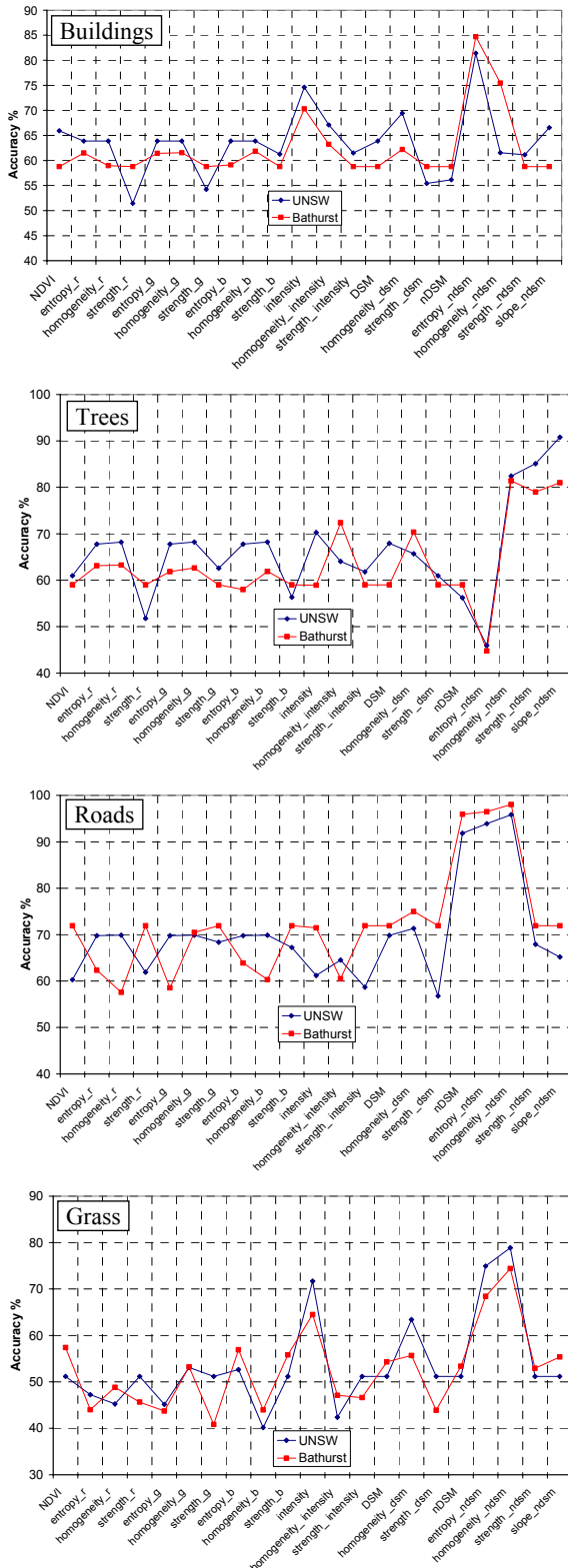


Figure 8. Contributions of the individual attributes to the quality of the classification results.

## 5.3 Evaluation of building results

Buildings as the most important features of the urban landscape were evaluated individually. First, building regions were retained if they were larger than the expected minimum building area (30 and 50m$^2$ for UNSW and Bathurst respectively) and/or were adjacent to a larger homogeneous region by a distance less than 1m. Finally, building borders were cleaned by removing structures that were smaller than 8 pixels and that were connected to the image border. In order to evaluate the classification accuracy, buildings were manually digitized in the multispectral images to serve as the reference data. Adjacent buildings that were joined but obviously separated were digitized as individual buildings. Otherwise, they were merged as one polygon. In comparison with the reference data 96% of all buildings were detected with well defined edges and also without holes. Also to give a good insight to the behaviour of the building detection process, *completeness* and *correctness* of detection results, described in (Rottensteiner et al., 2005), were computed and figure 9 shows these values for detected buildings. For the UNSW case study, buildings around 50m$^2$ were detected with completeness and correctness around 88% and 84% respectively and improving for increasing building size. For Bathurst case study, buildings around 30m$^2$ were detected with both completeness and correctness around 73% and 70% respectively and improving for increasing building size. For both cases, all buildings larger than 70m$^2$ were detected with both completeness and correctness over 90%. Similar accuracies have been reported in Rottensteiner *et al.* (2005). They evaluated a method for building detection by the Dempster-Shafer fusion of airborne laser scanner (ALS) data and multispectral images using different data sets. By Dempster-Shafer fusion, 95% of all buildings larger than 70m$^2$ were correctly detected.
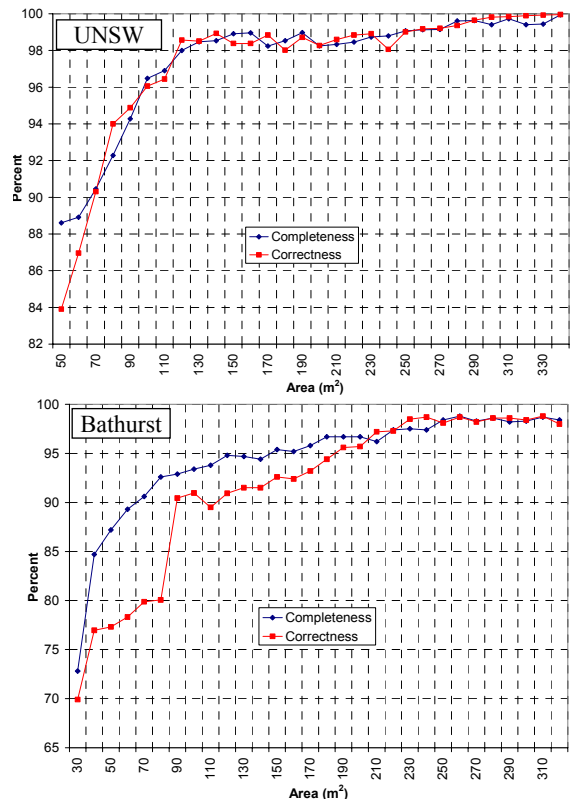


Figure 9. Completeness and correctness against building areas: for UNSW (top) and Bathurst (bottom).

## 6. CONCLUSION

A method for feature extraction based on Self-Organizing Map fusion of lidar, multispectral aerial images and 22 auxiliary attributes was presented. The attributes that were generated from the lidar data and multispectral images include: texture strength, Grey Level Co-occurrence Matrix (GLCM) homogeneity and entropy, Normalized Difference Vegetation Indices (NDVI) and slope. The approach significantly improves the accuracy of feature detection over approaches when only images and/or lidar data are used. The results show that using lidar data in the SOM improves the accuracy by 38% compared with using aerial photography alone, while using the generated attributes as well improve the result by a further 10%. An investigation into the contributions of the individual attributes showed that: entropy derived from nDSM performed the best for building detection; slope derived from nDSM performed the best for tree detection; homogeneity derived from nDSM performed the best for road detection; and homogeneity derived from nDSM performed the best for grass detection. In the future, we intend to construct a hybrid classifier based on multiple classifiers operating simultaneously to achieve a more effective and robust decision making process.

## REFERENCES

Abo Akel, N., Zilberstein, O. and Doytsher, Y., 2004. A Robust Method Used with Orthogonal Polynomials and Road Network for Automatic Terrain Surface Extraction from LIDAR Data in Urban Areas. *International Archives of Photogrammetry, Remote Sensing and Spatial Information Science,* Vol. 35, ISPRS 274-279.

Alharthy, A. and Bethel, J., 2002. Heuristic Filtering and 3d Feature Extraction from LIDAR Data. *ISPRS the International Achieves of the Photogrammetry, Remote Sensing and Spatial Information Sciences* Vol. XXXIV.

Axelsson, P., 2000. DEM Generation from Laser Scanner Data Using Adaptive TIN Models. *International Archives of Photogrammetry and Remote Sensing,* XXXIII, Part B3:85–92.

Brunn, A. and Weidner, U., 1998. Hierarchical Bayesian Nets for Building Extraction Using Dense Digital Surface Models. *ISPRS Journal of Photogrammetry & Remote Sensing,* 53(5), pp. 296–307.

Clausi, D. A., 2002. An Analysis of Co-Occurrence Texture Statistics as a Function of Grey-Level Quantization. *Canadian Journal of Remote Sensing*, vol. 28 no. 1 pp. 45-62.

Förstner, W. and Gülch, E., 1987. A Fast Operator for Detection and Precise Location of Distinct Points, Corners and Centres of Circular Features. *In ISPRS Intercommission Workshop*, pages 281–305, Interlaken.

Haralick, R.M., 1979. Statistical and structural approaches to texture. *Proceedings of the IEEE*, 67, pp. 786-804.

Hug, C., 1997. Extracting Artificial Surface Objects from Airborne Laser Scanner Data. In: Gruen, A., Baltsavias, E. P., Henricsson, O. (Eds.), Automatic Extraction of Man-Made Objects from Aerial and Space Images (II), *Birkhäuser Verlag*, Basel, pp. 203-212.

Hugo, C., Capao, L., Fernando, B. and Mario, C., 2007. Meris Based Land Cover Classification with Self-Organizing Maps: preliminary results, *EARSeL SIG Remote Sensing of Land Use & Land Cover*.

Jen-Hon, L. and Din-Chang, T., 2000. Self-Organizing Feature Map for multi-spectral spot land cover classification. *GIS development.net, AARS*, ACRS 2000.

Kohonen, T., 1990. The Self-Organizing Map. Proceedings of *the IEEE*, 78: 1464-80.

LI Y. and WU H., 2008. Adaptive Building Edge Detection by Combining LiDAR Data and Aeria Images. *The International Archives of the Photogrammetry, Remote Sensing and Spatial Information Sciences*. Vol. XXXVII. Part B1. Beijing 2008

Maas, H. and Vosselman, G., 1999. Two Algorithms for Extracting Building Model from Raw Laser Altimetry Data. *ISPRS Journal of photogrammetry and remote sensing*, 54 (2-3):153-163, 1999.

Matikainen, L., Kaartinen, H. and Hyyppä, J., 2007. Classification Tree Based Building Detection from Laser Scanner and Aerial Image Data. *ISPRS Workshop on Laser Scanning 2007 and SilviLaser 2007*, Espoo, September 12-14, 2007, Finland.

Rottensteiner, F., Summer, G., Trinder J., Clode S. and Kubik, K., 2005. Evaluation of a Method for Fusing Lidar Data and Multi-Spectral Images for Building Detection. In: Stilla U, Rottensteiner F, Hinz S (Eds) CMRT05. *IAPRS*, Vol. XXXVI, Part 3/W24 - Vienna, Austria, August 29-30, 2005.

Seto, K. and Liu, W., 2003. Comparing ARTMAP Neural Network with the Maximum-Likelihood Classifier for Detecting Urban Change. *Photogrammetric Engineering & Remote Sensing*, 69: 981-990.

Vesanto, J., Himberg, J., Alhoniemi E. and Parhankangas J., 2000. SOM Toolbox for Matlab 5. *Technical Report* A57, Helsinki University of Technology, Neural Networks Research Centre, Espoo, Finland.

Vögtle, T., Steinle, E., 2000. 3D Modelling of Buildings Using Laser Scanning and Spectral Information. In: *International Archives of Photogrammetry and Remote Sensing*, Amsterdam, the Netherlands, Vol. XXXIII, Part B3, pp. 927-934.

Whitman, D., K. Zhang, S.P. Leatherman, and W. Robertson, 2003. Airborne Laser Topographic Mapping: Application to Hurricane Storm Surge Hazards. Earth Sciences in the Cities (G. Heiken, R. Fakundiny, and J. Sutter, editors), *American Geophysical Union*, Washington DC, pp. 363–376.